Supporting Information

Light-induced Spatial Separation of Charges Toward Different Crystal Facets of Square-like WO_3

Huihua Gong, Ruirui Ma, Fang Mao, Kewei Liu, Hongmei Cao, Hongjian Yan*

College of Chemistry, Sichuan University, Chengdu 610064 (P.R. China)

Fax: 86-28-85221339; Tel: 86-1355-1341-892; E-mail:hjyan@scu.edu.cn

1.Experimental section

1.1 Preparation of catalysts

1.1.1 Fabrication of square-like WO_3 nanoplates

The square-like WO_3 nanoplates were prepared by the facile hydrothermal synthesis process. Typically，1.0 g of $Na_2WO_4 \cdot 2H_2O$ was dissolved in 20 mL deionized water under continuous stirring at room temperature, then hydrochloric acid solution (5-6mL, HCl : H_2O = 1 : 1 v/v) was dropwise added into the solution. After stirring for 30 minutes, the obtained yellow precipitate was collected by centrifugation, washed several times using distilled water to eliminate Cl^-, and then transferred into a 30mL of Teflon-lined stainless steel autoclave for hydrothermal treatment at 180 ºC for 24 h. After naturally cooled down to room temperature, the resultant solid was collected by centrifugation and washed with deionized water for several times, and then dried in air at 60ºC for more than 8 h.

1.1.2 Synthesis of Pt/WO_3 powders (0.5 wt%) by different methods.

(1) photoreduction method

0.500g of WO_3 powder was suspended in 200 ml aqueous methanol (10% in volume) containing appropriate amount of $H_2PtCl_6 \cdot 6H_2O$. The suspension was magnetically stirred in the dark for at least an hour to achieve adsorption/desorption equilibrium between WO_3 and the $[PtCl_6]^{2-}$ ions. Then the mixture was illuminated for 30 min with a Xe lamp after removing the dissolved oxygen completely. The product was centrifuged and thoroughly washed with deionized water and ethanol for several times. After dried at 60ºC for more than 8 h, the sample (denoted as Pt/WO_3-Ph) was obtained.

(2) the impregnation method （In ethanol phase）

The loading of Pt cocatalyst on WO_3 was performed by the impregnation method. Typically, 0.500 g of WO_3 powder was impregnated in 30 mL ethanol containing appropriate amount of H_2PtCl_6, followed by stirring for overnight in the dark. After evaporation of the solvent and drying in air at 60ºC for more than 8 h, the obtained powder was annealed at 350ºC in air for 1h (the sample was denoted as Pt/WO_3-Im).

(3) the chemical reduction methods

a、$NaBH_4$ or ascorbic acid as reductant

0.500 g of WO_3 powder and appropriate amount of H_2PtCl_6 were added to 30 mL of deionized water, followed by stirring for overnight in the dark. Subsequently, a freshly prepared solution of $NaBH_4$ (0.0626mol/L, 15mL) or ascorbic acid（0.00193M, 30mL）was added dropwise into the above suspension, and magnetically stirred for 2 h at room temperature or magnetically stirred at 80 °C for 6 h, respectively. The as-prepared samples were collected, washed with deionized water and ethanol for several times, and dried at 60ºC for more than 8 h and labeled as Pt/WO_3-NB and Pt/WO_3-Vc, respectively.

b、ethylene glycol as a reductant

Typically, 0.500 g of WO_3 powder and appropriate amount of H_2PtCl_6 were added into 30 mL of ethylene glycol, and the suspension was vigorously stirred for 12 h. Then, the mixed solution was refluxed under vigorous stirring at 120 °C for 4 h. After cooling to room temperature, the precipitate was collected by centrifuging, washed with deionized water and ethanol for several times, and dried at 60ºC for more than 8 h. The sample was labeled as Pt/WO_3-EG. For comparison, another sample was obtained as follows: appropriate amount of H_2PtCl_6 was dissolved into 30 mL ethylene glycol and magnetically stirred for a overnight in the dark. Then, the mixed solution was refluxed under vigorous stirring at 120 °C for 4 h. After cooling to room temperature, 0.500 g of WO_3 powder was then dispersed into the solution and was vigorously stirred for 72 h at room temperature. The resulting suspension was centrifuged, washed and finally dried at 60°C for more than 8 h. The as-prepared powder was denoted as Pt/WO_3-EG-C.

1.2 Photocatalytic reactions

The photocatalytic water splitting O_2 evolution reactions were performed in a top-irradiation reactor vessel connected to a glass closed gas circulation system. The evolved gases were analyzed by an online gas chromatograph equipped with a thermal conductivity detector(SPSIC, GC-102AT, argon carrier). Typically, 0.300 g of the as-prepared Pt/WO_3 was dispersed in 200 mL of 0.01 M aqueous $AgNO_3$ solution ($AgNO_3$ acts as the sacrificial reagent). Before irradiated by a 300 W Xe lamp without cutoff filter, the reaction mixture was evacuated for 1 h to completely remove air and establish the adsorption-desorption equilibrium between the solution and photocatalyst with a constant magnetic stirring. The temperature of the reaction solution was maintained at 283 K by a flow of cooling water during the reaction. The gas generated was analyzed every 1 h.

1.3 Characterization

Scanning electron microscope (SEM) images of the samples was performed with JSM-5900LV Scanning Electron Microscopy (SEM, JEOL, Japan). Transmission electron microscopy images (TEM), high-resolution (HR) TEM images of the samples were obtained on transmission electron microscope (TEM; Tecnai G2 F20 S-TWIN). Powder X-ray diffraction (XRD) patterns were obtained using a X-Pert Pro diffractometer with Cu Kα radiation (λ=1.5406 Å）at a scanning speed of 4° min^{-1}. The UV–vis diffuse reflectance absorption spectra (DRS) were recorded on a UV-Vis spectrophotometer (UV3600, Shimadzu) by using $BaSO_4$ as a reference. The PL spectra of the samples was carried out with a Hitachi F-7000 photoluminescence spectrophotometer (Hitachi F-7000) and the excitation wavelength was 230 nm. X-ray photoelectron spectroscopy (XPS) spectra were measured on a V4105 instrument (Thermo Electron, USA) with a Mn Ka radiation source.

2.Figures and captions

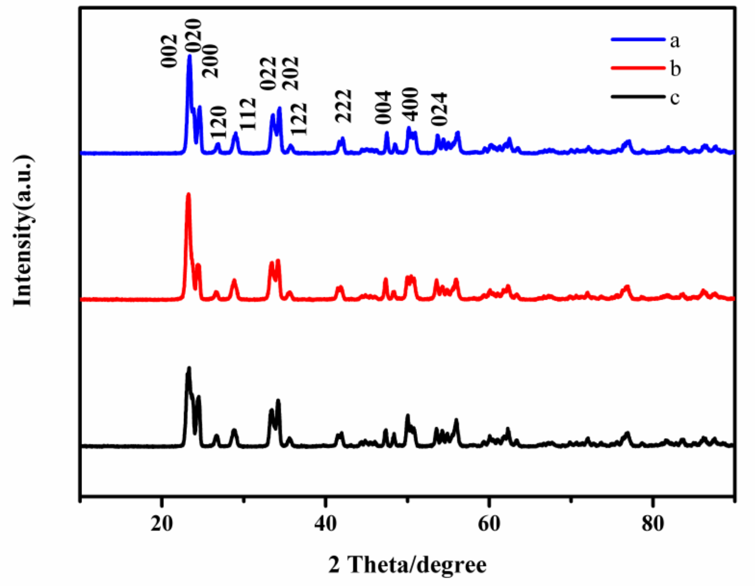

Figure S1. The X-ray diffraction (XRD) patterns of as-synthesized WO_3 (a), Pt/WO_3-Ph (b), and Pt/WO_3-EG (c).

The XRD pattern of the prepared catalysts are shown in Figure S1. The patterns clearly demonstrated that the pure WO_3 exhibits a monoclinic phase structure with obvious characteristic diffraction peaks at 2θ values of 23.146, 23.611, 24.369，33.302, and 34.189, corresponding to the (002), (020) ,(200), (022) and (202) planes, respectively (JCPDS No. 72-1465, a=7.300 Å, b=7.530 Å, and c=7.680 Å). In the XRD patterns of Pt/WO_3-EG, and Pt/WO_3-Ph samples, the diffraction peaks of Pt species could not be observed because of its low amount (0.5wt% Pt), small size and high dispersion on the square-like WO_3 nanoplates.

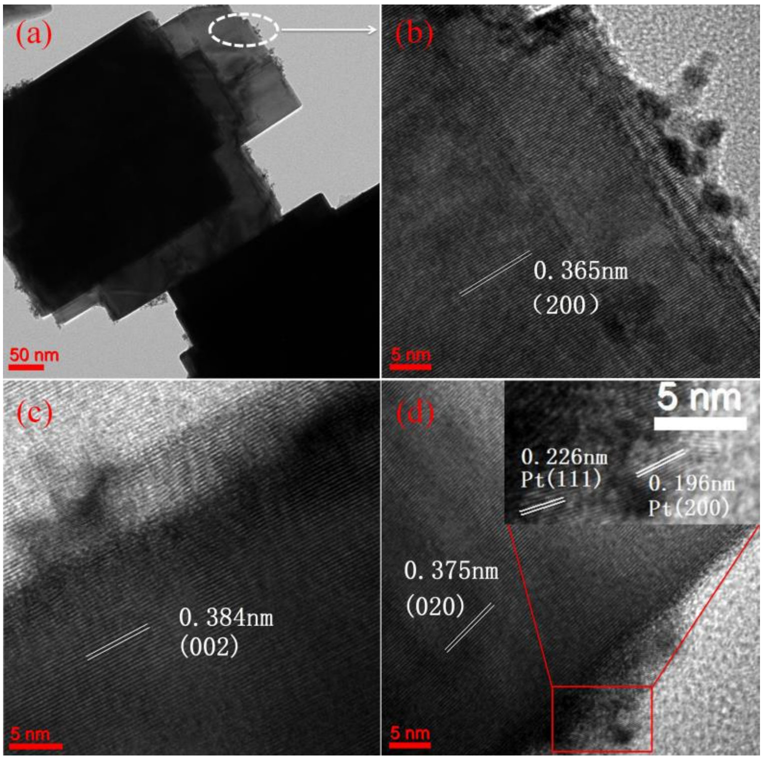

Figure S2. TEM and HRTEM images of Pt/WO_3-Ph.

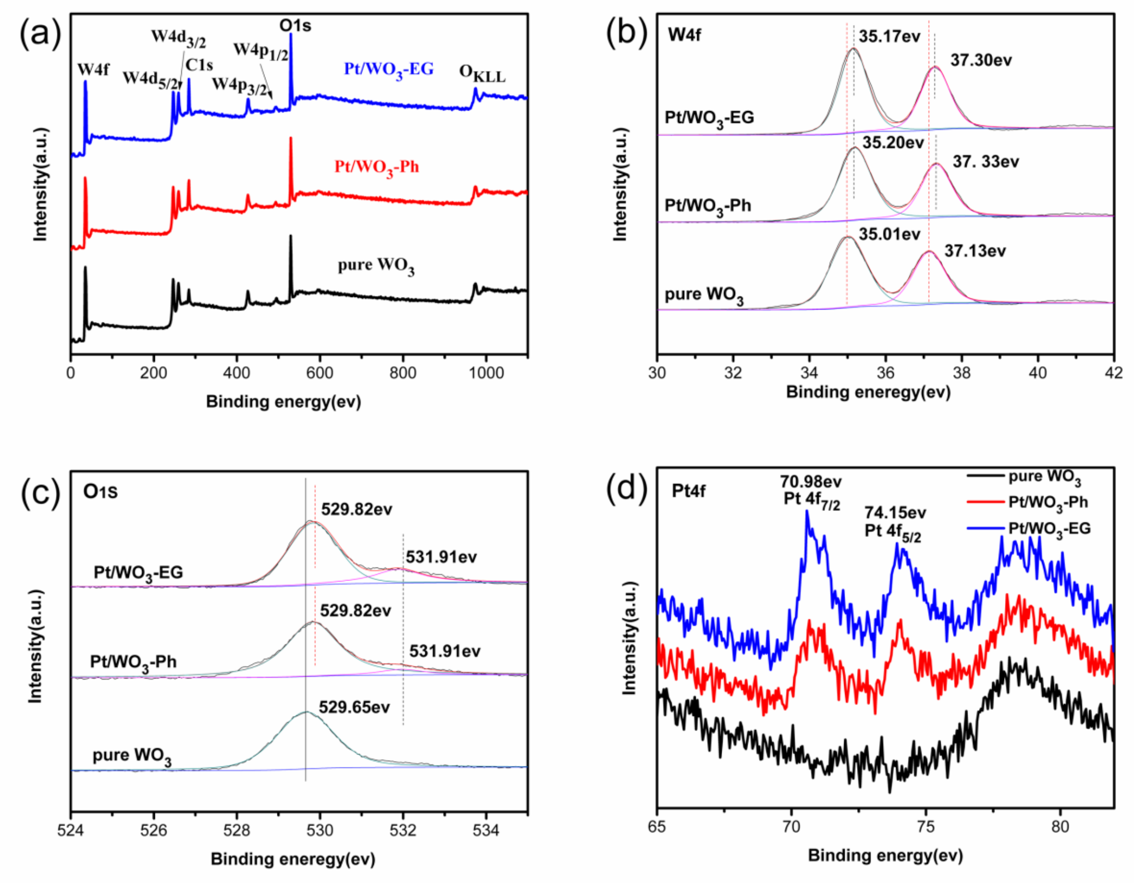

Figure S3. The XPS survey scan (a), and the corresponding high-resolution XPS spectra of W4f (b), O1s (c), and Pt4f (d) of WO_3, Pt/WO_3-Ph, and Pt/WO_3-EG samples.

The XPS survey scan (as shown in figure S3a) reveals the existence of the elements of W, O, C in the samples. The C 1s peak observed in the survey scan is due to the carbon contamination which was used to calibrate the binding energy. From Figure S3(b), the binding energy at around 35.01 and 37.13 eV can be ascribed to W $4f_{7/2}$ and W $4f_{5/2}$ respectively, suggesting that a W^{6+} oxidation state in the tungsten oxide sample[1]. The O1s peak(Figure S3 (c)) at 529.65 eV is associated with the lattice oxygen (W–O)(the oxide network) with O^{2-} states in WO_3, and the other O 1s peak at around 531.91 eV in the Pt/WO_3-Ph and Pt/WO_3-EG samples indicates the presence of surface adsorbed water molecule or surface hydroxide(−OH group) [1-5]. In addition, the binding energies at

70.98 and 74.15 eV in the Pt 4f spectrum of Pt/WO_3-Ph and Pt/WO_3-EG samples (Figure S3(d)) were well matched with Pt 4f $_{7/2}$ and 4f $_{5/2}$ electrons, respectively, [1, 6, 7] suggesting that the platinum species are predominately metallic Pt^0 form in both in the Pt/WO_3-Ph and Pt/WO_3-EG catalysts. Notably, compared to the pure WO_3 sample, the W 4f and O 1s peaks of Pt/WO_3-Ph and Pt/WO_3-EG samples show a small shift about 0.2ev toward high binding energy. As we know, In metal/metal oxide semiconductor systems, Pt metal is a well-known efficient co-catalyst for improving the catalytic activity of the WO_3 system, such a shift illustrating that strong interaction between Pt particles and the square-like WO_3, and photogenerated conduction band electrons tend to transfer from WO_3 to Pt nanoparticles , this thus leads to efficient charge separation which can reduce the photogenerated charge carriers recombination rate and exhibits high activity for O_2 evolution.[8,9]

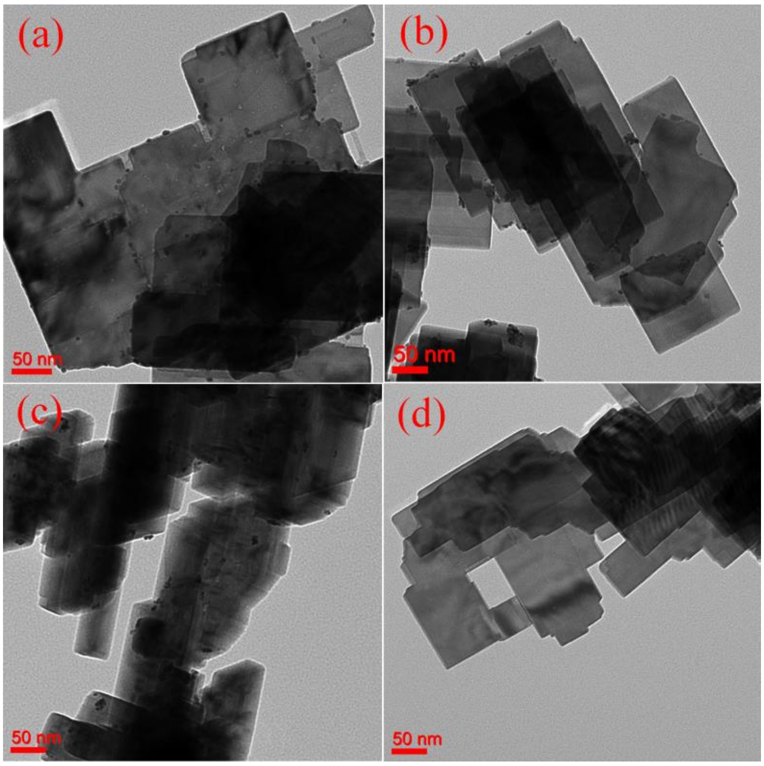

Figure S4. TEM images of Pt/WO_3-Im (a), Pt/WO_3- NB (b and c), and Pt/WO_3- Vc (d).

TEM image of the Pt/WO_3-Im sample prepared by traditional impregnation method (Figure S4 (a)) shows that the Pt nanoparticles with relatively large particles of 5-10 nm exhibit uniform distributions on the different crystal faces of the square-like WO_3, including (200), (020) and (002) surfaces. The TEM images of Pt/WO_3-NB are given in Figure S4 (b) and (c). Figure S4 (b) shows most of Pt particles with a average particle size of around 4-5 nm are mainly deposited on the minor facets and aggregate together seriously on the surface of square-like WO_3, while a small amount of Pt particles loaded on the dominant facet are near the edges. Furthermore, the morphology of some square-like tungsten trioxide was destroyed due to the alkaline condition (Figure S4(c)). Figure S4(d) shows that Pt nanoparticles can not be deposited on the surfaces of square-like WO_3 by using ascorbic acid as a reductant. These results indicate that the loading methods have effect on the location, dispersion and particle size of platinum nanoparticles on the surfaces of square-like WO_3.

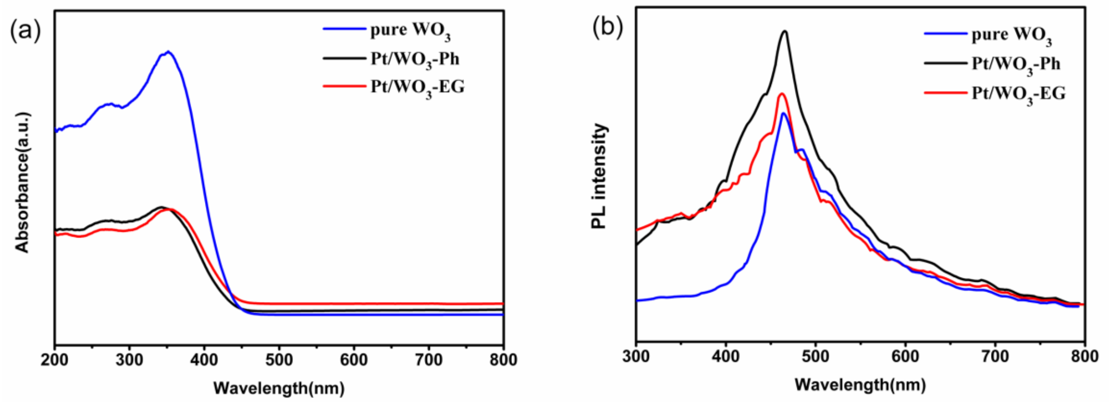

Figure S5. UV−vis diffuse reflectance spectra (a), PL spectra (b) of WO_3, Pt/WO_3-Ph and Pt/WO_3-EG.

The UV−vis diffuse reflectance spectra indicate that the loading of Pt on the square-like WO_3 did not obviously change its absorption range. However, the absorption intensity was significantly weakened due to that the Pt particles shadow the photocatalyst absorbing the light.[10] As shown in Figure S5 (b), the PL intensity of the Pt/WO_3-EG is lower than that of Pt/WO_3-Ph, which indicates lower recombination rate of photo-generated electron-hole pairs in Pt/WO_3-EG. The decreasement of electron-hole recombination rate in Pt/WO_3-EG might be ascribed to that Pt cocatalyst loaded on different facets of WO_3 could accelerate transfer of the electron and hole on the surfaces of square-like WO_3.

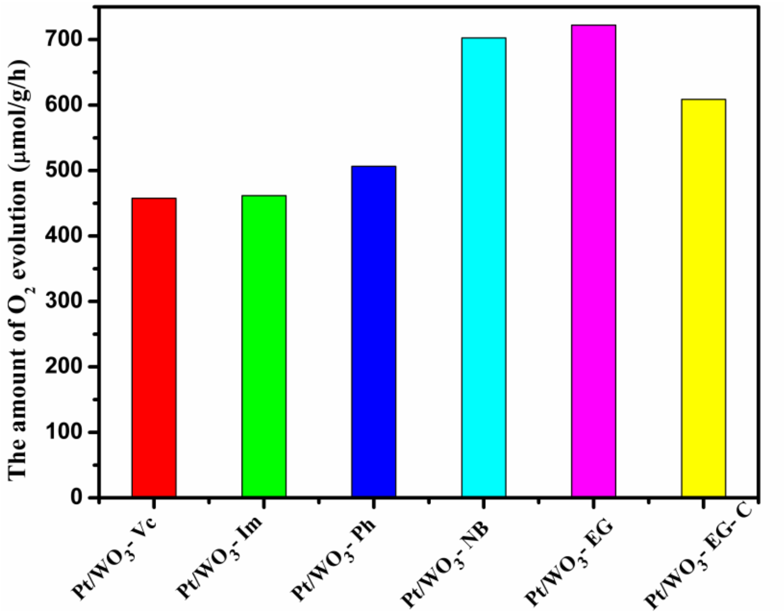

Figure S6. Photocatalytic performances of Pt/WO_3 prepared by different methods.

It clearly illustrate that the deposition method of Pt nanoparticle has effect on photocatalytic water oxidation activity. The Pt/WO_3-EG prepared by the ethylene glycol reduction method exhibited higher O_2 evolution rate than that of Pt/WO_3 samples prepared by other methods. The photocatalytic O_2 evolution rate on Pt/WO_3-EG and Pt/WO_3-Im is 722.2 μmol·g^{-1}·h^{-1} and 461.8 μmol·g^{-1}·h^{-1}, respectively. TEM images of Pt/WO_3-EG(Figure 2(c)) and Pt/WO_3-Im(Figure S4) show that the Pt particles of these two samples were randomly dispersed on both of the minor edged facets (002) and (020) and the main (200) facets of square-like WO_3 nanoplates. However, there are differences in particle size of Pt loaded on the two samples. The average Pt particle size of Pt/WO_3-Im (around 5-10 nm) is larger than that of Pt/WO_3-EG sample (2-3nm). These results indicated that particle size of Pt nanoparticles has affect on the photocatalytic activity of photocatalyst and the enhanced photocatalytic O_2 evolution rate of Pt/WO_3-EG could be ascribed to the smaller particle size of platinum nanoparticles.

The photocatalytic O_2 evolution rate on Pt/WO_3-NB is 702.7 μmol·g^{-1}·h^{-1}, slightly lower than that on Pt/WO_3-EG(722.2 μmol·g^{-1}·h^{-1}). As we know, WO_3 will significantly occur corrosion phenomenon at pH >4[11]. In Figure S4(b) and (c), it can be observed that the morphology of some square-like tungsten trioxide is destroyed due to alkaline solution of sodium borohydride, which will result in the greater specific surface area of WO_3.

The O_2 evolution rate on Pt/WO_3-Ph(506.5 μmol·g^{-1}·h^{-1}) slightly higher than that of Pt/WO_3-Vc(457.8 μmol·g^{-1}·h^{-1}). This result indicates that Pt loaded on the minor facets cannot improve the photocatalytic activity of WO_3 significantly. Furthermore, it is notable that the O_2 evolution rate on Pt/WO_3-Ph (506.5 μmol·g^{-1}·h^{-1}) is much lower than that of Pt/WO_3-EG(722.2 μmol·g^{1}·h^{-1}). Considering the dispersion and the location of Pt nanoparticles of these two samples, the results above strongly indicate that the location of Pt nanoparticles on the facets of square-like WO_3 nanoplates has more influence on photocatalytic activity than the particle size of platinum nanoparticles. That is, the square-like WO_3 with Pt loaded mainly on dominant (200) facets shows higher photocatalytic activity than that Pt deposited on the minor facets.

The photocatalytic O_2 evolution rate on Pt/WO_3-EG-C is 608.8 μmol·g^{-1}·h^{-1}, which is lower than that on Pt/WO_3-EG (722.2 μmol·g^{-1}·h^{-1}). For the Pt/WO_3-EG, Pt nanoparticles were loaded on the square-like WO_3 at high temperature treatment leads to tightly-bound Pt particles on WO_3. For the Pt/WO_3-EG-C, the reduced Pt particles were loaded on the surfaces of square-like WO_3 by physical adsorption at room temperature, which lead to the weak adhesion of Pt particles onto the WO_3 surfaces. (Whereas the weak adhesion of reduced Pt particles onto the WO_3 surface at room temperature contains loosely-bound Pt particles in Pt/WO_3-EG-C). The strong interaction between Pt and WO_3 for the Pt/WO_3-EG facilitates the migration of the photogenerated electron-holes from WO_3 to Pt, which leads to efficient charge separation and exhibits high performance for O_2 evolution.[12]

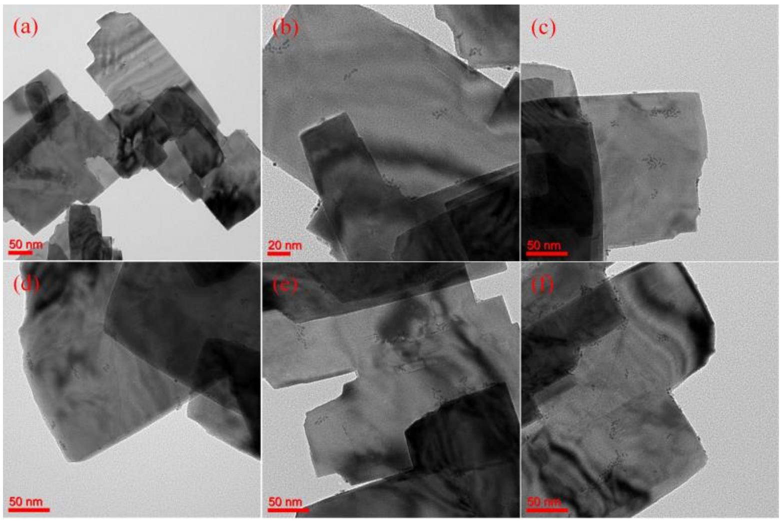

Figure S7. TEM images of Pt/WO_3-EG (a-f).

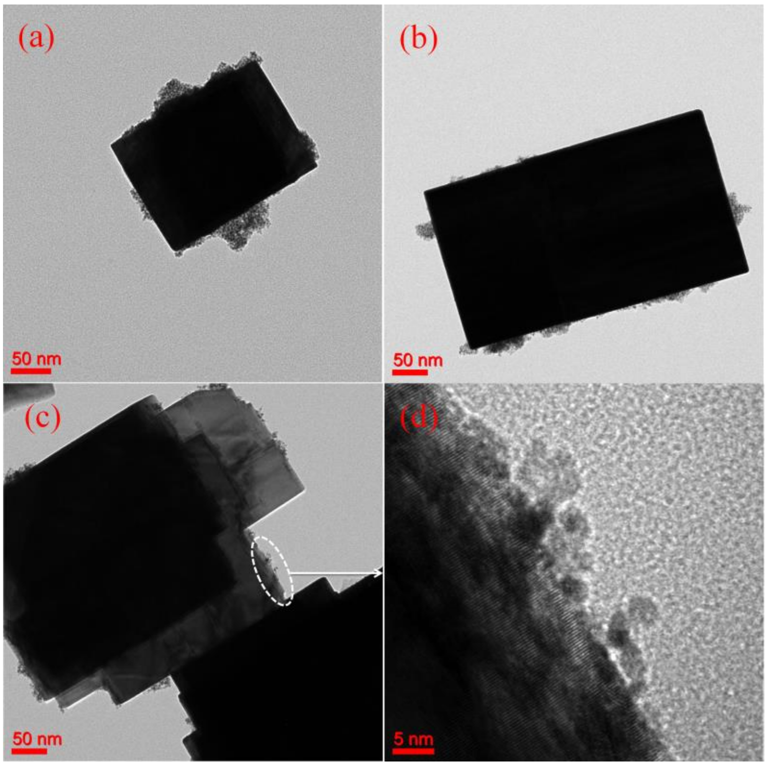

Figure S8. TEM images (a-c) and HRTEM image (d) of Pt/WO_3-Ph.

TEM images of Pt/WO_3-EG and Pt/WO_3-Pt are shown in Figure S7 and Figure S8, respectively. As shown in Figure S7, in the samples of Pt/WO_3-EG, the Pt nanoparticles were mainly deposited on the dominant (200) facets of square-like WO_3 nanoplates. For Pt/WO_3-Ph, the negatively charged $[PtCl_6]^{2-}$ were adsorbed preferentially on positively charged edged facets prior to photodeposition, and then be reduced to Pt loaded on the edged facets of square-like WO_3 nanoplates by photogenerated electrons under irradiation. From the TEM results, it seems that the overall loading amount of platinum in Pt/WO_3-EG is relatively lower than that in Pt/WO_3-Ph. The higher loading amount of Pt nanoparticles in Pt/WO_3-Ph was the result of synergetic effect of the facet-dependent adsorption of the Pt precursor and surface photo-reduction of $[PtCl_6]^{2-}$ by photogenerated electrons on the edged facets (light-induced the preferred migration of photo-generated electrons to the edged facets).

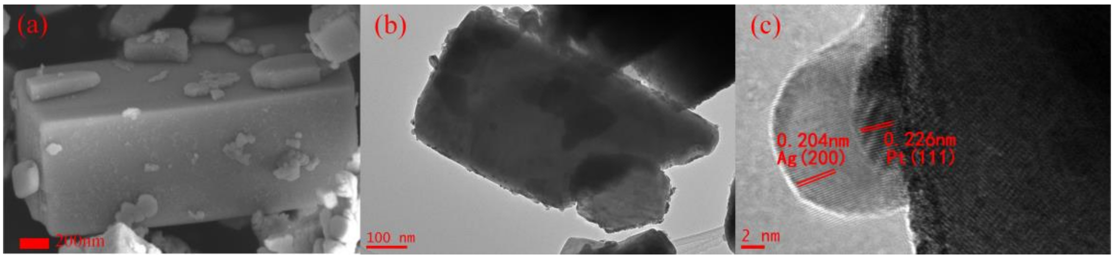

Figure S9. SEM image (a), TEM (b) and HRTEM (c) images of Pt/WO_3-EG after irradiation 1h in the presence of $AgNO_3$ as electron sacrifice agent.

Figure S9 (a) and (b) show that most particles are deposited on the edged facets of the square-like WO_3, while few particles are deposited on the dominant facets of the square-like WO_3. Figure S9(c) demonstrates that some nanoparticles loaded on the edged facets with particle size of around 20 nm are Ag. Furthermore, compared the TEM and SEM images of Pt/WO_3-EG after irradiation 1h with that after irradiation 0.5h (shown in Figure 4), the amount and the particle size of particles deposited on the edged facets of the square-like WO_3 increase with the irradiation time. This result also confirm that the reduction process of Ag^+ by photogenerated electrons took place on the corresponding minor facets of the square-like WO_3.

References for supporting materials

1 Z. Wen, W. Wu, Z. Liu, H. Zhang, J. Li and J. Chen, *Phys. Chem. Chem. Phys*., 2013, 15, 6773-6778.

2 F. Zhan, R. Xie, W. Li, J. Li, Y. Yang, Y. Li and Q. Chen, *RSC Adv*., 2015, 5, 69753-69760.

3 B. Weng, J. Wu, N. Zhang and Y. J. Xu, *Langmuir*, 2014, 30, 5574-5584.

4 Y. Kong, H. Sun, X. Zhao, B. Gao and W. Fan, *Appl. Catal. A. Gen.*, 2015, 505, 447-455.

5 I. Aslam, C. Cao, W. S. Khan, M. Tanveer, M. Abid, F. Idrees, R. Riasat, M. Tahir, F. K. Butt and Z. Ali, *RSC Adv*., 2014, 4, 37914.

6 J. Zeng and J. Lee, *J. Power Sources*, 2005, 140, 268-273.

7 W. J. Ong, L. L. Tan, S. P. Chai and S. T. Yong, *Dalton Trans*., 2015, 44, 1249-1257.

8 Y.M.Wu, H.B.Liu, J.L.Zhang, F.Chen, *J. Phys. Chem. C*, 2009, 113, 14689-14695.

9 L. Jia, D. A. Bulushev, O. Y. Podyacheva, A. I. Boronin, L. S. Kibis, E. Y. Gerasimov, S. Beloshapkin, I. A. Seryak, Z. R. Ismagilov and J. R. H. Ross, *J. Catal.*, 2013, 307, 94-102.

10 C.Young, TM.Lim, K.Chiang, J.Scott, R.Amal, *Appl. Catal., B*, 2008, 78, 1-10.

11 K. Wenderich, A. Klaassen, I. Siretanu, F. Mugele and G. Mul, *Angew. Chem., Int. Ed.*, 2014, 53, 12476-12479.

12 Y. Shiraishi, Y. Kofuji, S. Kanazawa, H. Sakamoto, S. Ichikawa, S. Tanaka and T. Hirai, *Chem. Commun.*, 2014, 50, 15255-15258.